ACS APPLIED MATERIALS & INTERFACES

Research Article

www.acsami.org

PEG-Phospholipids Coated Quantum Rods as Amplifiers of the Photosensitization Process by FRET

Reut Timor,[†] Hana Weitman,[*,†] Nir Waiskopf,[‡] Uri Banin,[*,‡] and Benjamin Ehrenberg[†]

[†]Department of Physics and Institute of Nanotechnology and Advanced Materials, Bar Ilan University, Ramat Gan 52900, Israel

[‡]Institute of Chemistry and Center for Nanoscience and Nanotechnology, The Hebrew University of Jerusalem, Jerusalem 91904, Israel

Supporting Information

ABSTRACT: Singlet oxygen ($^1O_2$) generated upon photostimulation of photosensitizer molecules is a highly reactive specie which is utilized in photodynamic therapy. Recent studies have shown that semiconductor nanoparticles can be used as donors in fluorescence resonance energy transfer (FRET) process to excite attached photosensitizer molecules. In these studies, their unique properties, such as low nanoscale size, long-term photostability, wide broad absorbance band, large absorption cross section, and narrow and tunable emission bands were used to provide advantages over the traditional methods to produce singlet oxygen. Previous studies that achieved this goal, however, showed some limitations, such as low FRET efficiency, poor colloidal stability, nonspecific interactions, and/or complex preparation procedure. In this work, we developed and characterized a novel system of semiconductor quantum rods (QRs) and the photosensitizer meso-tetra(hydroxyphenyl) chlorin (*m*THPC), as a model system that produces singlet oxygen without these limitations. A simple two-step preparation method is shown; Hydrophobic CdSe/CdS QRs are solubilized in aqueous solutions by encapsulation with lecithin and PEGylated phospholipid (PEG−PL) of two lipid lengths: PEG_{350} or PEG_{2000}. Then, the hydrophobic photosensitizer *m*THPC, was intercalated into the new amphiphilic PEG−PL coating of the QR, providing a strong attachment to the nanoparticle without covalent linkage. These PEGylated QR (eQR)−*m*THPC nanocomposites show efficient FRET processes upon light stimulation of the QR component which results in efficient production of singlet oxygen. The results demonstrate the potential for future use of this concept in photodynamic therapy schemes.

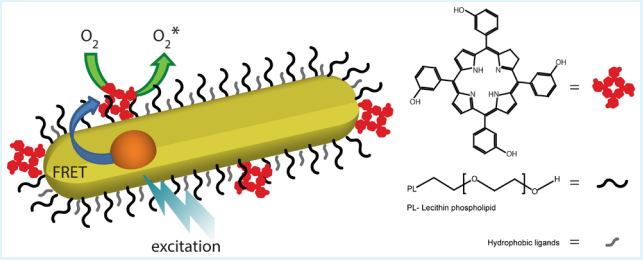

KEYWORDS: *quantum rods, photosensitizer, fluorescence resonance energy transfer, nanocomposites, singlet oxygen, PEGylated phospholipid coating*

INTRODUCTION

Photodynamic therapy (PDT) is currently an approved FDA therapy for cancer. It takes advantage of the interaction between light, a photosensitizing agent, and oxygen to initiate selective destruction of a target tissue by localized generation of cytotoxic singlet oxygen.[1−8] The photophysical process of singlet oxygen generation during PDT involves a photosensitizer, mostly tetrapyrrole derivatives, such as porphyrins and chlorins, that have a suitable wavelength at which it can be excited from S_0 to S_1, following which the excitation energy is transduced by intersystem crossing to excite oxygen to singlet oxygen ($^1O_2$).[5−8]

meso-Tetra(hydroxyphenyl) chlorin (*m*THPC), is a second generation photosensitizer which is currently considered the most potent and clinically used photosensitizer.[1,9−13] *m*THPC has a high quantum yield of singlet oxygen generation. However, like most photosensitizers, it has poor solubility in water, which leads to its aggregation in aqueous solutions and to rapid disappearance of its photochemical activity. Moreover, *m*THPC has two main narrow absorbance bands and a small absorption cross section, which requires intense illumination in very specific wavelengths in order to achieve singlet oxygen generation.

Semiconductor nanoparticles (SC-NPs) have attracted great interest over the past few years, and were used in various biomedical applications ranging from imaging, sensing, and drug delivery to light stimulation of neurons.[14−21] For example, semiconductor quantum dots (QDs) conjugated to delivery agents were used to stain cancer cells both in vitro and in animal models.[14−17] SC-NPs can present unique photophysical characteristics, such as size tunable emission, large absorption cross section, wide absorbance band, long-term photostability, and high fluorescence quantum yields.[22−27] These properties make them ideal to be used as donors in fluorescence resonance energy transfer (FRET). This fact did not go without notice, stimulating researchers to explore combination of SC-NPs with photosensitizers for use in PDT.

Received: May 25, 2015
Accepted: September 3, 2015
Published: September 3, 2015

DOI: 10.1021/acsami.5b04318
ACS Appl. Mater. Interfaces 2015, 7, 21107−21114

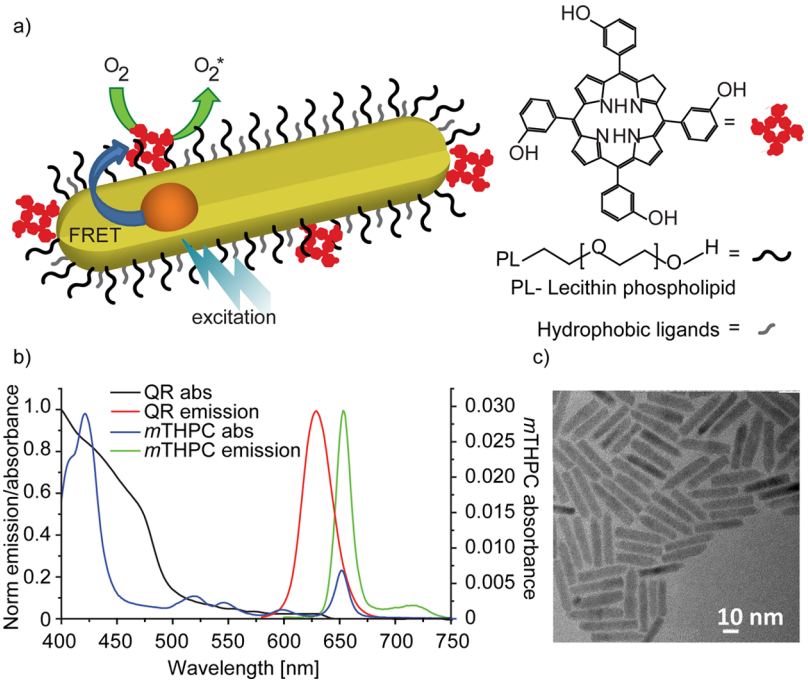

Figure 1. (a) Illustration of eQR−*m*THPC nanocomposite system for $^1O_2$ production. Excitation of the semiconductor, results in FRET from the CdSe core to the *m*THPC molecules intercalated to the PEG−PL coating, which results in singlet oxygen production. (b) Normalized absorbance and emission spectra of CdSe/CdS QRs in hexane (black and red curves, respectively) and *m*THPC in THF (blue and green). The graph emphasizes the larger absorption cross section of QRs in comparison to *m*THPC, and the good spectral overlap between QRs emission and *m*THPC absorption. (c) TEM image showing good size distribution of QRs, 32 ± 2 nm in length and 6 ± 0.5 in diameter.

Burda and co-workers presented SC-NPs as potential PDT agents.[28] They linked CdSe QDs to silicon phthalocyanine PC 4 (PC4) and determined a 77% FRET efficiency. Although QD-PC4 conjugates showed excellent ability to generate singlet oxygen, it worked only in organic solutions, and thus was not suitable for biological applications. Follow up works have shown the ability to use additional nanocomposites of QDs and photosensitizers to produce singlet oxygen, some of them producing it also in aqueous environments.[28−36] These works proved the advantages in the use of QD−photosensitizer nanocomposites for PDT, confirming the ability to induce apoptosis in cancer cells, while presenting long-term photostability and higher light sensitivity.

Beyond this progress, the different systems that were suggested still presented some limitations such as, poor colloidal stability and/or relatively low FRET efficiency in biological solutions, pH = 7.4 buffers with strong ionic strength. The major reason for these limitations is nonideal SC-NP surface coating, such as bifunctional ligands (e.g., thiolate ligands)[14,37] or polymers[14,37−41] that increases the distance of the photosensitizer from the emitting core and/or not providing significant steric stability to the NP. Moreover, some of the used surface coatings were shown to cause nonspecific interactions between NPs and cells.[42]

In this study, we propose a new SC-NP−photosensitizer nanocomposites for singlet oxygen production which is based on hydrophobic semiconductor quantum rods (QR) covered with PEG-Phospholipids (eQR) and *m*THPC intercalated into the resulting amphiphilic coating (see Figure 1a). We characterize the size and morphology of the eQR and present efficient FRET between the eQR and *m*THPC, which results in efficient singlet oxygen generation in aqueous solutions. This signifies the potential for future application of such architectures also in PDT schemes.

MATERIALS AND METHODS

The phospholipids: 1,2-dipalmitoyl-*sn*-glycero-3-phospho-ethanolamine-*N*-[methoxy(polyethylene glycol)-2000] and 1,2-dipalmitoyl-*sn*-glycero-3-phosphoethanolamine-*N*-[methoxy (polyethylene glycol)-350] (PEG_{2000} and PEG_{350}) were purchased from Avanti Polar Lipids (Alabaster, Alabama, U.S.A.). *meso*-Tetra (hydroxyphenyl) chlorin (*m*THPC) was obtained from Prof. Mathias O. Senge, SFI Tetrapyrrole Laboratory, University of Dublin, Ireland. The singlet oxygen chemical quencher 9,10-dimethylanthracene (DMA), hexane and L-*α*-phosphatidylcholine (L-*α*-lecithin), from frozen egg yolk, were purchased from Sigma-Aldrich (St. Louis, Missouri, U.S.A.). Solvents such as THF, DMF, and chloroform were purchased from Alfa Aesar (Ward Hill, Massachusetts, U.S.A.).

Nanoparticles Synthesis. CdSe/CdS core/shell seeded nanorods were synthesized following a previously described protocol based on a seeded growth approach.[43] Briefly, CdSe seeds were synthesized by fast injection of selenium dissolved in trioctylphosphine (TOP) solution into a four-neck flask containing CdO in trioctylphosphine oxide (TOPO) and *n*-octadecylphosphonic acid (ODPA) at 350 °C under an argon atmosphere. The crude solution was then washed to remove excess ligands. Seed concentration was calculated based on absorption measurements and was mixed with elemental sulfur dissolved in TOP. Then the CdSe seeds and sulfur in TOP solution was rapidly injected into a four-neck flask containing TOPO, ODPA, CdO, and hexylphosphonic acid at 360 °C. After cooling, the crude solution was dissolved in toluene, and methanol was added to precipitate the NPs and remove excess precursors and ligands.

Spectroscopic Measurements. Absorbance spectra were measured with a Shimadzu (Kyoto, Japan) UV-2501PC UV−visible spectrophotometer. The fluorescence intensity, excitation and emission spectra, anisotropy, and time-drive kinetic measurements were all measured with a Cary Eclipse fluorimeter, model 1.12 (Agilent Technologies, Santa Clara, California, U.S.A.) equipped with a polarizer accessory. Fluorescence lifetime measurements were carried

DOI: 10.1021/acsami.5b04318
ACS Appl. Mater. Interfaces 2015, 7, 21107−21114

out using a fluorescence spectrometer (Edinburgh Instruments FLS920) after irradiating the sample 475 ± 5 nm. Fluorescence QY values were measured using the Hamamatsu absolute photoluminescence quantum yield spectrometer C11347 quanturus.

Preparations of eQR. Colloidal suspension of PEG−PL coated QR was produced by modification of previously described method.[44] For encapsulation of 1.25 mg/mL eQR, 0.5 mg QR in hexane was mixed with 1.42 mg lecithin solution in chloroform and 1.39 mg PEG_{350} or 3.56 mg PEG_{2000}. The molar ratio of PEG_{2000} or $-PEG_{350}$ to lecithin was 40% and 60%, respectively.[44] The mixture was dispensed into a 20 mL scintillation vial and was subjected to a stream of blowing nitrogen until all the solution had evaporated (40−60 min), forming a dry layer at the bottom of the vial. Finally, 400 μL of distilled water was added, and the sample was vortexed for few seconds.

Binding Kinetics. Kinetic experiments were performed by adding 8 μM *m*THPC to eQR (50 μg/mL). The *m*THPC's fluorescence intensity increased while keeping the solution agitated on a shaker for 10−12 h until it reached an equilibrium point.

Binding Constants. The binding constant, K_b, was calculated using a titration method.[45] Solutions containing 8 μM *m*THPC and increased concentrations of eQR dissolved in phosphate buffer saline (PBS), were prepared. The samples were excited at 633 nm and emission spectra were measured from 643 to 700 nm. Then the maximal intensities (F) were plotted against the eQR concentration (L), and the results were fitted to eq 1 (Origin, Microcal Software, Northampton, Massachusetts, U.S.A.).

$$F(L) = \frac{F_{init} + F_{comp}K_b[L]}{1 + K_b[L]} \quad (1)$$

where F_{init} and F_{comp} are the initial fluorescence intensity of the *m*THPC without eQR, and the fluorescence obtained asymptotically at complete binding, respectively. K_b is obtained in units of $(\mu g/mL)^{-1}$.

Preparation of eQR−*m*THPC Nanocomposites. In order to expedite the intercalation of the *m*THPC to the eQR, for FRET and $^1O_2$ generation measurements, a slightly modified procedure was used in which the encapsulation of the QR and intercalation of the photosensitizer to the PEG−PL coating is performed concomitantly. A mixture of phospholipids, PEG phospholipids, QR, and *m*THPC, were all dissolved in chloroform. Then the chloroform was evaporated with a gentle stream of nitrogen, forming a dry film (60 min). PBS was added, and the solution was vortexed for few seconds.

FRET Measurements. A known approach of steady-state emission measurement was used, exciting the QR (donor) and detecting the light emitted by the donor and the acceptor (*m*THPC); when FRET occurs, the donor emission decreases, and the decay time shortens. A series of vials were prepared with increasing quantities of *m*THPC (0−8 μM), and a constant concentration of eQR (6.5 μg/mL). Steady state measurements were performed using excitation at 580 nm. Fluorescence lifetime measurements were performed using 475 nm as the excitation wavelength, and the emission decay was followed at 620 nm (Donor's only). Kinetic time-resolved FRET experiments were performed by adding 8 μM *m*THPC to eQR_{350} and eQR_{2000}, while keeping the solution agitated on a shaker for 24 h. FRET efficiencies were calculated using the ratio between the fluorescence intensities and the decay lifetime of the donor in presence and absence of the acceptor[46] (F_{DA} and F_D, and τ_{DA} and τ_D, respectively).

$$E = 1 - \frac{F_{DA}}{F_D} = 1 - \frac{\tau_{DA}}{\tau_D} \quad (2)$$

Singlet Oxygen Generation Efficiency Measurements. Samples were prepared concomitantly by adding 8 μM *m*THPC, 13 μg QR, 40% PEG−PL, and 60% phospholipid molar ratio, evaporated under nitrogen, and dissolved in 2 mL PBS, as described above. The irradiation sources for photosensitization measurements of eQR, eQR−*m*THPC nanocomposites were measured using 473 and 650 nm laser diode (Lasever Inc. Ningbo, China). The laser beam was transferred to the top of the sample cuvette in the fluorimeter with an optical diverging lens (LC1582-A, D = 25.4 mm, F = −75 mm ThorLabs Newton, New Jersey, U.S.A.) to obtain uniform irradiation along the sample cuvette. The laser beam passes the sample cuvette through the long axis, perpendicularly to the excitation and emission channels directions of the fluorimeter. The intensity of the laser beam (3−6 mW) was measured, before and after the measurements, with a laser powermeter (model PD2-A, Ophir, Jerusalem, Israel). To measure the production yield of singlet oxygen, we employed 9,10-dimethylanthracene (DMA, 2 μM final concentration) as a chemical target that photo-oxidized rapidly by singlet oxygen. The irradiation initiated only after reaching the binding equilibrium of the hydrophobic DMA which intercalate into the lipid-PEG coating. The DMA was excited at 376 nm, and the decreasing fluorescence intensity at 405 nm was monitored over time. To evaluate the singlet oxygen generation efficiency, φ_Δ, the following equations were used,[47] where DMA concentration (T) as a function of time (t) is given by the following:

$$\ln T = \ln T_0 + \frac{\varphi_\Delta}{k_s} \times A \times (1 - 10^{-OD}) \times (e^{-k_s \times t} - 1) \quad (3)$$

where T_0 is the initial DMA concentration, A is the power of the laser, k_s is the decay rate of the sensitizer's concentration, due to self-destruction, and OD is the optical density of the solution in the laser diode excitation wavelength. For measuring the QR singlet oxygen production yield, since the sensitizer is stable, eq 3 evolves into the usual formula (see Supporting Information, SI, for further details also on error analysis):

$$T = T_0 \times e^{-\varphi_\Delta \times A \times (OD \times 2.3) \times t} \quad (4)$$

Electron Microscopy. The size and morphology of the synthesized QR were assessed by TEM (Tecnai G2 Spirit Twin T-12), HR-TEM (JEOL−TEM 2100 (LaB6)) and EDS−Thermo-Fisher, Si-Dry detector, equipped with Noron six software. The size and morphology of the coated particles (eQR_{350} and eQR_{2000}) were assessed by HRSEM−STEM (Magellan 400, FEI), at an accelerating voltage of 5 and 25 kV, with current of 0.2- 0.8 nA; using detector STEM II, mode: bright field.

Anisotropy Measurements. Continuous illumination with monochromatic polarized light was used to excite our photosensitizer−*m*THPC system which is embedded into the lipid−PEG micelles. The anisotropy is an indication of the rotational freedom of the molecule in the viscous medium, the PEG−PL coating in our case. Steady state anisotropy (r_0) was measured for *m*THPC in glycerol as control, and for *m*THPC embedded in the eQR_{350} and eQR_{2000}.

RESULTS AND DISCUSSION

CdSe/CdS seeded nanorods (QRs) were chosen as the SC-NP model system, which could ultimately be replaced in a more biocompatible SC-NP. The rod geometry of the SC-NPs, that was not examined so far for singlet oxygen production was proven to show advantages over the QDs geometry in different applications;[18,48,49] They have a larger extinction coefficient, making them more light sensitive, they present higher fluorescent quantum yield, due to lower reabsorption and significantly reduced FRET interactions with neighboring QR, they have larger surface area which allows their conjugation to multiple molecules, for example, both delivery agents and photosensitizers, etc. Moreover, QRs show similar and even better FRET efficiency to conjugated dyes in comparison to QDs, depending the geometry of the seed.[49]

Figure 1b presents the absorption and emission spectra (red and black curve, respectively) and Figure 1c presents transmission electron micrograph (TEM) of the QR. The dimensions of the nanorods are 32 ± 2 nm in length and 6 ± 0.5 nm in diameter. High resolution TEM and energy-dispersive X-ray spectroscopy (EDS) were also used and confirmed the CdSe/CdS structure (SI). The QR show lower absorption beyond 480 nm, attributed mostly to the CdSe seed,

DOI: 10.1021/acsami.5b04318
ACS Appl. Mater. Interfaces 2015, 7, 21107−21114

with a sharp rise at 480 nm, resulting from the significant additional absorption of the CdS rod. The emission peak of the QRs is at 629 nm and their measured fluorescence quantum yield is 50% in hexane.

Characterization of the PEGylated Nanoparticles. The QRs were synthesized in organic solvents; therefore, to solubilize the hydrophobic QRs in aqueous solution, we encapsulated the nanoparticles into micelles consisting of polyethylene glycol−phospholipids (PEG−PL) using modification of previously described methods.[44] This method was chosen trying to solve the limitations of the QDs' surface coatings used so far for PDT. For example, this technique is known to produce water-soluble nanocomposites with higher colloidal stability than ligand exchange with thiolated ligands. Moreover, using this surface coating we utilize the known PEG advantages to increase NPs biocompatibility and minimize nonspecific interactions with cells and biological molecules.[42,50,51]

The QRs were coated with a mixture of lecithin with two lengths of PEG−PL: either PEG_{350} or PEG_{2000}—composed of 7 and 44 ethylene glycol monomers, respectively. The encapsulated QRs (eQR_{350} and eQR_{2000}) presented identical emission and excitation spectra to those before the encapsulation. The fluorescence quantum yield in aqueous solution was 54.5%. This emphasizes the advantage of the encapsulation method, since the traditional ligand exchange techniques to render SC-NPs soluble in aqueous solutions, usually resulting in significant decreases in their fluorescence quantum yield.

For defining the size of the encapsulated QRs, we used STEM measurements with a low voltage. The average size of the eQR_{350} and eQR_{2000} was 36/9.5 and 42/16 nm, respectively (Figure 2). Therefore, the coating diameters, which are the length of the entangled PEG chains, are approximately, 2 and 5 nm. The calculated lengths of stretched PEG_{350} and PEG_{2000} chains are 2.9 and 17 nm. Therefore, the measured lengths of the PEG chains are shorter than the calculated ones, indicating as expected that the PEG chains are folded.

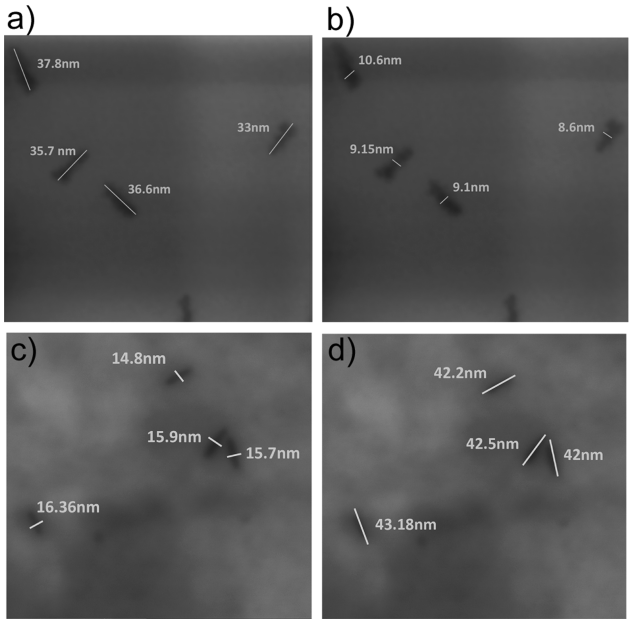

Figure 2. STEM images of eQR: (a,b) The measured length and width of eQR_{350}. (c,d) The measured length and width of eQR_{2000}. The synthesized nanorod sizes were increased by coating diameters of 2 and 5 nm for eQR350 and eQR_{2000}, respectively.

The encapsulation transforms the hydrophobic QR to a colloidal solution of PEG−lipid coated QR in water. Every single QR is trapped in a micelle in a way that the lipid embeds the hydrophobic QR as the amphiphilic PEG chains extend outward in the aqueous medium. Hydrophobic small molecules can easily penetrate into the micelle by noncovalent interactions. This was exploited to achieve close proximity to the photosensitizer molecules, which is of great importance to allow an efficient FRET process without compromising on the colloidal stability. This is in comparison to polymer surface coatings, which usually increase NP colloidal stability, while increasing the distance of the conjugated molecules from the semiconductor surface.

The hydrophobic *m*THPC, which is a powerful, clinically relevant, frequently used photosensitizer, was chosen for our model system. The main absorbance peaks of *m*THPC are at 420 and 650 nm and its emission peak in THF is located at 652 nm (Figure 1b). When examining the absorption coverage of both eQR and *m*THPC in the same concentration and in the whole region between 320 and 800 nm, the integrated eQR spectrum is larger by more than 2 orders of magnitude in comparison to *m*THPC (The molar extinctions of QR and *m*THPC in the visible spectral range differ by 2 orders of magnitude. For example, the molar extinction coefficients at 420 nm, wherein the most significant peaks of *m*THPC are $\varepsilon = 1.59 \times 10^7\ M^{-1}cm^{-1}$ vs $\varepsilon = 1.44 \times 10^5\ M^{-1}cm^{-1}$ for QR and *m*THPC, respectively). This great difference is emphasized in Figure 1b, signifying the ability of SC-NP−photosensitizer nanocomposites to increase the light sensitivity of photosensitizer based systems for singlet oxygen production. Using a noncoherent white light will exploit both the high light harvesting capability of the QR in the visible light region and the mTHPC's excellent singlet oxygen production efficiency, and thus will undoubtedly enhance the efficiency of the photochemical reaction that underlies PDT. Figure 1b also illustrates the good overlap that exists between the eQR emission and the excitation spectrum of *m*THPC, which is a fundamental requirement for efficient FRET. We calculated the overlap integral (J) and the Forster radius (R_o), for the two PEG chain lengths (SI). $J(\lambda)$ for eQR_{350} and eQR_{2000} is $(6.3 \pm 1.4) \times 10^{-14}\ M^{-1}\cdot cm^3$. The evaluated R_0 obtained for eQR_{350}−*m*THPC and eQR_{2000}−*m*THPC, is 4.3 ± 0.1 nm. This evaluated R_0 is a consequence of the good spectral overlap and the CdSe/CdS QR high fluorescence quantum yield of the donor in water (54.5%).

Binding Constants. The binding constant (K_b) between *m*THPC and the eQRs was measured by a titration method.[40] Solutions with increased concentrations of eQR were mixed with 8 μM *m*THPC, and emission spectra were measured after excitation of eQRs. An enhancement in the *m*THPC emission maxima was observed as a function of eQRs concentration (Figure 3). The K_b constants were then extracted by fitting eq 1 to the results. The calculated K_b constant for eQR_{350} and eQR_{2000} is 2.6 ± 0.6 $(nM)^{-1}$, indicating the achievement of strong noncovalent binding between *m*THPC and the eQR. These results also allow extraction of the eQR concentration required to achieve 50% binding of 8 μM *m*THPC. The concentration is $1/K_b = 0.4 \pm 0.1$ nM for eQR_{350} and eQR_{2000}.

FRET Efficiency. The intercalation of the *m*THPC to the eQR afforded indirect excitation of *m*THPC by FRET. Excitation of solutions containing eQR mixed with increased

DOI: 10.1021/acsami.5b04318
ACS Appl. Mater. Interfaces 2015, 7, 21107−21114

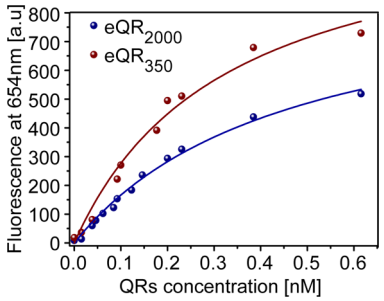

Figure 3. Fluorescence intensity of *m*THPC at 654 nm, as a function of eQR concentrations. The binding constants extracted from these curves indicate the achievement of strong noncovalent binding between eQR and the *m*THPC.

concentrations of *m*THPC at 580 nm resulted in increased emission of *m*THPC (Figure 4a). Excitation in 580 nm is not optimal for eQRs; however, it is convenient for the study of FRET in our system, since *m*THPC has no absorption in this wavelength. Excellent FRET efficiencies, up to 94%, were estimated for both PEG_{2000} and PEG_{350} coated QR-*m*THPC nanocomposites (Figure 4b). As far as we know, this is one of the highest FRET efficiencies demonstrated so far for SC-NP–photosensitizer nanocomposites in aqueous solutions. We assume that the high efficiencies derive from the good spectral overlap, donor's high fluorescence quantum yield, and the close proximity between the QR and the *m*THPC, as achieved using our PEGylation route.

Lifetime Measurements. Another confirmation for these observations was realized using lifetime measurements. Samples were excited at 580 nm, and emission was detected at 620 nm where the *m*THPC has minimal emission. In the presence of *m*THPC, a drastic shortening of the decay time is observed (Figure 4c, red and black versus green and blue). The effective decay lifetimes ($\langle\tau\rangle$), the times required to reach to 1/e of the initial signal, are summarized in Table 1, and confirm the assumed FRET mechanism. The effective lifetimes with and without *m*THPC were then used for calculating FRET efficiency for eQR_{350}–*m*THPC and eQR_{2000}–*m*THPC nanocomposites eq 2, presenting high quantum yields of 95% and 92%, similar to those presented using the fluorescence values.

Table 1. Effective Decay Lifetime ($\langle\tau\rangle$) for eQR and eQR–*m*THPC Nanocomposites PEGylated Concomitantly[a]

PEG_n		$\langle\tau\rangle$ [nsec]
PEG_{350}	eQR	13.1 ± 0.1
	eQR–*m*THPC	0.7 ± 0.1
PEG_{2000}	eQR	12.6 ± 0.1
	eQR–*m*THPC	1 ± 0.1

[a]The table demonstrates the shortening of the effective lifetime in the presence of *m*THPC which confirm the assumed FRET process, between the eQR and *m*THPC. $\langle\tau\rangle$ refers to the time required to reach to 1/e of the initial signal.

Kinetic time-resolved FRET experiments were also performed. The decay times were measured in several time points following the addition of the *m*THPC photosensitizer, showing shortening lifetimes with time due to the accumulation of *m*THPC molecules into the eQR coating. The results are consistent with increasing concentrations of *m*THPC in the steady state fluorescence FRET experiment (Figure 4a). The effective lifetimes $\langle\tau\rangle$ are presented in Table 2.

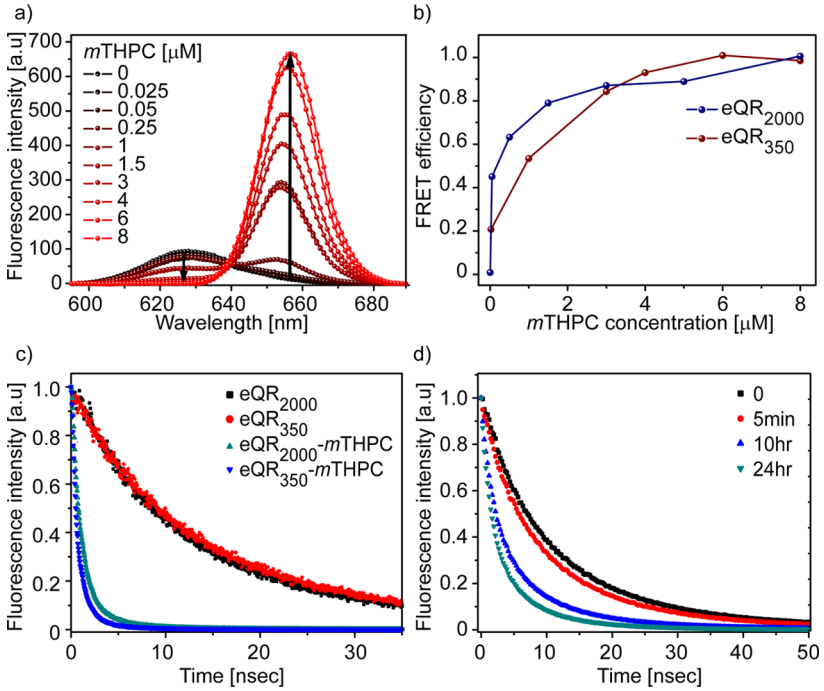

Figure 4. (a) The change in the fluorescence intensities of eQR_{2000} and *m*THPC upon addition of *m*THPC due to FRET. The emission of the eQR is reduced, whereas that is of *m*THPC is increased. (b) Energy transfer efficiency for both types of coated QR as a function of *m*THPC concentration. The FRET efficiency is increased with *m*THPC concentrations until a maximal efficiency of almost 1 is achieved. (c) Fluorescence lifetime measurements with and without *m*THPC (eQR–*m*THPC PEGylated concomitantly) showing significant shortening of the eQRs in the presence of *m*THPC. (d) Kinetic fluorescence lifetime measurements with eQR_{350} reveal that the eQRs lifetime is shortening with time upon addition of *m*THPC.

DOI: 10.1021/acsami.5b04318
ACS Appl. Mater. Interfaces 2015, 7, 21107–21114

Table 2. Effective Decay Lifetime (<τ>) for eQR-*m*THPC Nanocomposites Measured during Sensitizer's Intercalation to the eQR Coating[a]

eQR	time	⟨τ⟩ [nsec]
eQR_{350}	0 h	10.5 ± 0.1
	5 min	6.1 ± 0.1
	10 h	3.9 ± 0.1
	24 h	2.4 ± 0.1
eQR_{2000}	0 h	11.9 ± 0.1
	5 min	8.5 ± 0.1
	10 h	7.6 ± 0.1
	24 h	5.3 ± 0.1

[a]The table shows the kinetics of the process and proves the shortening of the effective lifetime results from the FRET process and not from the presence of *m*THPC in the solution. ⟨τ⟩ refers to the time required to reach to 1/e of the initial signal.

Singlet Oxygen Quantum Yield. Proving an efficient FRET process, we then continued to examine the efficiency of singlet oxygen generation. Kinetic measurements of singlet oxygen production were done by monitoring the fluorescence decay of the sensing molecule DMA (Figure 5). The quantum yield of the singlet oxygen production was then calculated for each measurement, and the results are summarized in Table 3.

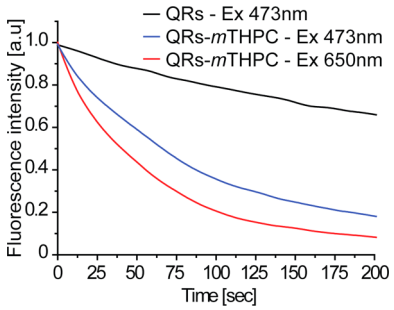

Figure 5. DMA fluorescence disappearance as a result of singlet oxygen generation following excitation of eQR at 473 nm (black), *mTHPC in eQR–mTHPC* composite *at Ex650 nm* (red) and eQR–*m*THPC at 473 nm (blue).

Table 3. Singlet Oxygen Generation Efficiencies[a]

φ_Δ/PEG_n	PEG_{2000}	PEG_{350}
φ_Δ eQR (473 nm)	0.32 ± 0.02	0.15 ± 0.01
φ_Δ eQR–*m*THPC(650 nm)	0.8 ± 0.02	1 ± 0.04
φ_Δ eQR–*m*THPC(473 nm)	0.79 ± 0.02	0.75 ± 0.02

[a]The results are relative to the highest efficiency evaluated.

The first set of measurements were detection of singlet oxygen formation in the presence of eQR alone during excitation at 473 nm (Figure 5 black curve, Table 3, row 1). These results exhibit higher photosensitization efficiency for the eQR_{2000} than the eQR_{350}. The results are explainable on the basis of $^1O_2$'s diffusion in different thicknesses of the PEG–PL layers, PEG_{2000} or PEG_{350}. Singlet oxygen is generated by the QR and diffuses through the PEG–PL coating. When the chemical target used is DMA, the probability of $^1O_2$ to react with the delocalized target is higher if the diffusion path of the oxygen originates from a deeper location within the membrane.[52] Therefore, the extended time $^1O_2$ stays in the PEG_{2000} layer in comparison to PEG_{350} results in higher photosensitization efficiency.

The *m*THPC self-singlet oxygen efficiency was measured by excitation of the eQR–*m*THPC nanocomposites at 650 nm, which matches the *m*THPC absorbance spectrum where eQR has no absorption at all. A higher photosensitization efficiency is given for *m*THPC when it penetrates into the eQR_{350} PEG–PL layer compared to eQR_{2000} (Figure 5 red curve, Table 3, row 2). These apparently contradicting findings are explainable when measuring the anisotropy of *m*THPC in both types of nanocomposites.

The steady state anisotropy measured for *m*THPC in glycerol, as control, is 0.27 and for *m*THPC embedded in the eQR_{350} and eQR_{2000} are 0.17 and 0.08, respectively. The anisotropy is an indication of the rotational freedom of the molecule in the viscous medium, the PEG–PL coating in our case. The lower anisotropy measured for *m*THPC molecules embedded in eQR_{2000} in comparison to eQR_{350} indicates higher rotational freedom in the PEG_{2000}–PL layer. This facilitates internal conversion as a competing process and, therefore, lower photosensitization efficiency of *m*THPC embedded in eQR_{2000}.

The singlet oxygen generation efficiency for eQR–*m*THPC via FRET process was measured by excitation of the eQR–*m*THPC nanocomposite at 473 nm that matches mainly the eQR absorbance spectrum (Figure 5 blue curve, Table 3, row 3). Faster decay is seen in comparison to excitation of eQRs alone (black curve). The results emphasize the singlet oxygen production by the eQR–*m*THPC nanocomposite via FRET on levels compared to the production upon direct irradiation of *m*THPC alone.

The similarity of $^1O_2$ generation efficiencies was seen for both eQR_{350}–*m*THPC and eQR_{2000}–*m*THPC nanocomposites. This can be explained considering the two opposite contributions that are described above, the dwell time of $^1O_2$ and the anisotropy of *m*THPC in both layers.

CONCLUSIONS

In this paper, we present and characterize novel encapsulated QR–photosensitizers nanocomposites for efficient singlet oxygen production. Strong non-covalent binding was demonstrated between hydrophobic CdSe/CdS seeded QR encapsulated by PEG–PL and lecithin and hydrophobic *m*THPC molecules. For both eQR_{350}–*m*THPC and eQR_{2000}–*m*THPC nanocomposites an enormous FRET efficiency was observed (94%). This indicates that in parallel to the known achievement of very good colloidal stability in physiological solutions using this encapsulation technique and the minimization of nonspecific interaction with biological molecules and cells realized by the PEG, the method suggested here also allows for achieving excellent FRET efficiencies. This was contributed to the use of SC-NP with rod geometry, the maintenances of large fluorescent quantum yield after the phase transfer and the ability of the *m*THPC to penetrate deep into the PEG–PL coating close to the QR surface.

The high FRET efficiency of the nanocomposite eQR–*m*THPC indicates the possibility for overall use of the wide light bandwidth of the eQR via FRET, in parallel to the ability to directly excite the *m*THPC. This kind of approach may bring a more efficient generation of singlet oxygen by the nanocomposite than by the *m*THPC alone.

Comparison between eQR_{350}–*m*THPC nanocomposites to eQR_{2000}–*m*THPC nanocomposites has shown similar results in

DOI: 10.1021/acsami.5b04318
ACS Appl. Mater. Interfaces 2015, 7, 21107–21114

the fluorescence and FRET parameters and in the $^1O_2$ generation efficiencies; however, the sizes of the particles are smaller for eQR_{350} compared to eQR_{2000}. For further investigation in cells, one should consider using the smallest particles which will penetrate more easily into cells.

This introduction of photochemical, colloidally stable, and efficient singlet oxygen producing systems, together with the ability to utilize other SC-NPs properties to add functionalities to the nanocomposites, such as for imaging, delivery, etc., will hopefully yield in the development of a better toolkit for cancer therapy.

■ ASSOCIATED CONTENT

Supporting Information

This material is available at The Supporting Information is available free of charge on the ACS Publications website at DOI: 10.1021/acsami.5b04318.

Characterization of the NPs and estimation of the Förster distances (PDF)

■ AUTHOR INFORMATION

Corresponding Authors

*E-mail: Hana.weitman@mail.biu.ac.il (H.W.).
*E-mail: banin@chem.ch.huji.ac.il (U.B.).

Funding

This work was supported by the Michael David Falk Chair in Laser Phototherapy.

Notes

The authors declare no competing financial interest.

■ ACKNOWLEDGMENTS

We thank Qlight Nanotech for providing nanorod samples. We thank Dr. Judith Grinblat for the help with HRTEM images and Katya Gotlib for the help with HRSEM images. N.W. thanks Clara Robert for a predoctoral Einstein Fellowship. U.B. thanks the Alfred & Erica Larisch memorial chair.

■ DEDICATION

In memory of Professor Benjamin Ehrenberg, who passed away on July 19, 2015. Vice President of Research at Bar-Ilan university, and a member of the Department of Physics and the Nano Medicine Center at the Institute of Nanotechnology and Advanced Materials (BINA). Ever since he established a biophysics research group at BIU in 1980, Professor Ehrenberg has applied optical techniques to study systems of biological and medical interest. In his latest works, he used nanoparticles as a vehicle for delivering anticancer drugs and for activating those drugs with light.

■ ABBREVIATIONS

PEG−PL, poly(ethylene glycol)−phospholipid
QD, quantum dots
QR, quantum rods
eQR, encapsulated quantum rods
eQR_{350}, PEG_{350} encapsulated quantum rods
eQR_{2000}, PEG_{2000} encapsulated quantum rods
$^1O_2$, singlet oxygen
*m*THPC, *meso*-tetra(hydroxyphenyl) chlorin
SC-NP, Semiconductor nanoparticles

■ REFERENCES

(1) Dougherty, T. J.; Gomer, C. J.; Henderson, B. W.; Jori, G.; Kessel, D.; Korbelik, M.; Moan, J.; Peng, Q. Photodynamic Therapy. *J. Natl. Cancer Inst.* **1998**, *90*, 889−905.
(2) Weishaup, K. R.; Gomer, C. J.; Dougherty, T. J. Identification of Singlet Oxygen as the Cytotoxic Agent in Photoinactivation of a Murine Tumor. *Cancer Res.* **1976**, *36*, 2326−2329.
(3) Dougherty, T. J. Photosensitizers: Therapy and Detection of Malignant Tumors. *Photochem. Photobiol.* **1987**, *45*, 879−889.
(4) Morris, R. L.; Azizuddin, K.; Lam, M.; Berlin, J.; Nieminen, A.; Kenney, M. E.; Samia, A. C. S.; Burda, C.; Oleinick, N. L. Fluorescence Resonance Energy Transfer Reveals a Binding Site of a Photosensitizer for Photodynamic Therapy. *Cancer Res.* **2003**, *63*, 5194−5197.
(5) Lower, S. K.; El-Sayed, M. A. The Triplet State and Molecular Electronic Processes in Organic Molecules. *Chem. Rev.* **1966**, *66*, 199−241.
(6) El-Sayed, M. A. The Triplet State: Its Radiative and Nonradiative Properties. *Acc. Chem. Res.* **1968**, *1*, 8−16.
(7) *Molecular Spectroscopy of the Triplet State*; McGlynn, S. P., Azumi, T., Kinoshita, Eds.; Prentice-Hall: Englewood Cliffs, NJ, 1969.
(8) DeRosa, M. C.; Crutchey, R. J. Photosensitized Singlet Oxygen and its Applications. *Coord. Chem. Rev.* **2002**, *223−234*, 351−371.
(9) Van Geel, P. J.; Oppelaar, H.; Oussoren, Y. G.; Der Van Valk, M. A.; Stewart, F. A. Photosensitizing Efficacy of MTHPC-PDT Compared to Photofrin-PDT in the RIF1Mouse Tumour and Normal Skin. *Int. J. Cancer* **1995**, *60*, 388−394.
(10) Copper, M. P.; Tan, I. B.; Oppelaar, H.; Ruevekamp, M. C.; Stewart, F. A. mTHPC mediated Photodynamic Therapy for Early Oral Squamous Cell Carcinoma. *Arch. Otolaryngol., Head Neck Surg.* **2003**, *129*, 709−711.
(11) Senge, M. O.; Brandt, J. C. Temoporfin (foscan(R), 5,10,15,20-Tetra(mhydroxyphenyl) Chlorin) − A Second-Generation Photosensitizer. *Photochem. Photobiol.* **2011**, *87*, 1240−96.
(12) Berlanda, J.; Kiesslich, T.; Engelhardt, V.; Krammer, B.; Plaetzer, K. Comparative In Vitro Study on the Characteristics of Different Photosensitizers Employed in PDT. *J. Photochem. Photobiol., B* **2010**, *100*, 173−80.
(13) Mitra, S.; Foster, T. H. Photophysical Parameters, Photosensitizer Retention and Tissue Optical Properties Completely Account for the Higher Photodynamic Efficacy of Meso-Tetra-Hydroxyphenyl-Chlorin vs Photofrin. *Photochem. Photobiol.* **2005**, *81*, 849−859.
(14) Bruchez, M.; Moronne, M.; Gin, P.; Weiss, S.; Alivisatos, A. P. Semiconductor Nanocrystals as Fluorescent Biological Labels. *Science* **1998**, *281*, 2013−2016.
(15) Jaiswal, J. K.; Mattoussi, H.; Mauro, J. M.; Simon, S. M. Long-Term Multiple Color Imaging of Live Cells Using Quantum Dot Bioconjugates. *Nat. Biotechnol.* **2003**, *21*, 47−51.
(16) Gao, X.; Cui, Y.; Levenson, R. M.; Chung, L. W. K.; Nie, S. In Vivo Cancer targeting and Imaging with Semiconductor Quantum Dots. *Nat. Biotechnol.* **2004**, *22*, 969−976.
(17) Michalet, X.; Pinaud, F. F.; Bentolila, L. A.; Tsay, J. M.; Doose, S.; Li, J. J.; Sundaresan, G.; Wu, A. M.; Gambhir, S. S.; Weiss, S. Quantum Dots for Live Cells, In Vivo Imaging, and Diagnostics. *Science* **2005**, *307*, 538−544.
(18) Tran, P. T.; Goldman, E. R.; Anderson, G. P.; Mauro, J. M.; Mattoussi, H. Use of Luminescent CdSe-ZnS Nanocrystal Bioconjugates in Quantum Dot-Based Nanosensors. *Phys. Status Solidi B* **2002**, *229*, 427−432.
(19) Medintz, I. L.; Clapp, A. R.; Mattoussi, H.; Goldman, E. R.; Fisher, B.; Mauro, J. M. Self-Assembled Nanoscale Biosensors Based on Quantum Dot FRET Donors. *Nat. Mater.* **2003**, *2*, 630−638.
(20) Medintz, I. L.; Clapp, A. R.; Brunel, F. M. Proteolytic Activity Monitored by Fluorescence Resonance Energy Transfer Through Quantum Dot-Peptide Conjugates. *Nat. Mater.* **2006**, *5*, 581−589.
(21) Bareket, L.; Waiskopf, N.; Rand, D.; Lubin, G.; David-Pur, M.; Ben-Dov, J.; Roy, S.; Eleftheriou, C.; Sernagor, E.; Cheshnovsky, O.; Banin, U.; Hanein, Y. Semiconductor Nanorod−Carbon Nanotube

DOI: 10.1021/acsami.5b04318
ACS Appl. Mater. Interfaces 2015, 7, 21107−21114

Biomimetic Films for Wire-Free Photostimulation of Blind Retinas. *Nano Lett.* **2014**, *14*, 6685−6692.
(22) Alivisatos, A. P. Perspectives on the Physical Chemistry of Semiconductor Nanocrystals. *J. Phys. Chem.* **1996**, *100*, 13226−13239.
(23) Bawendi, M. G.; Steigerwald, M. L.; Brus, L. E. The Quantum Mechanics of Larger Semiconductor Clusters ("Quantum Dots"). *Annu. Rev. Phys. Chem.* **1990**, *41*, 477−496.
(24) Burda, C.; Chen, X.; Narayanan, R.; El-Sayed, M. A. Chemistry and Properties of Nanocrystals of Different Shapes. *Chem. Rev.* **2005**, *105*, 1025−1102.
(25) Hines, M.; Guyot-Sionnest, P. Synthesis and Characterization of Strongly Luminescent ZnS-Capped CdSe Nanocrystals. *J. Phys. Chem.* **1996**, *100*, 468−471.
(26) Weller, H. Colloidal Semiconductor Q-particles: Chemistry in the Transition Region between Solid State and Molecules. *Angew. Chem., Int. Ed. Engl.* **1993**, *32*, 41−53.
(27) Murray, C. B.; Norris, D. J.; Bawendi, M. G. Synthesis and Characterization of Nearly Monodisperse CdE (E 5 Sulfur, Selenium, Tellurium) Semiconductor Nanocrystallites. *J. Am. Chem. Soc.* **1993**, *115*, 8706−8715.
(28) Samia, A. C. S.; Chen, X.; Burda, C. Semiconductor Quantum Dots for Photodynamic Therapy. *J. Am. Chem. Soc.* **2003**, *125*, 15736−15737.
(29) Shi, L. X.; Hernandez, B.; Selke, M. Singlet Oxygen Generation from Water-Soluble Quantum Dot-Organic Dye Nanocomposites. *J. Am. Chem. Soc.* **2006**, *128*, 6278−6279.
(30) Hsieh, J. M.; Ho, M. L.; Wu, P. W.; Chou, P. T.; Tsai, T. T.; Chi, Y. Iridium-Complex Modified CdSe/ZnS Quantum Dots; A Conceptual Design for Bifunctionality Toward Imaging and Photosensitization. *Chem. Commun.* **2006**, *6*, 615−617.
(31) Tsay, J. M.; Trzoss, M.; Shi, L. X. Singlet Oxygen Production by Peptide-Coated Quantum Dot-Photosensitizer Conjugates. *J. Am. Chem. Soc.* **2007**, *129*, 6865−6871.
(32) Ma, J.; Chen, J. Y.; Idowu, M.; Nyokong, T. Generation of Singlet Oxygen via the Composites of Water-Soluble Thiol-Capped CdTe Quantum Dots − Sulfonated Aluminum Phthalocyanines. *J. Phys. Chem. B* **2008**, *112*, 4465−4469.
(33) Bakalova, R.; Ohba, H.; Zhelev, Z. Quantum Dot Anti-CD Conjugates: Are They Potential Photosensitizers or Potentiators of Classical Photosensitizing Agents in Photodynamic Therapy of Cancer? *Nano Lett.* **2004**, *4*, 1567−1573.
(34) Lei, L.; Jin-Feng, Z.; Nayoun, W.; Ho, J.; Sungjee, K.; Ji-Yao, C. Quantum Dot-Aluminum Phthalocyanine Conjugates Perform Photodynamic Reactions to Kill Cancer Cells via fluorescence Resonance Energy Transfer. *Nanoscale Res. Lett.* **2012**, *7*, 386.
(35) Zenkevich, E. I.; Sagun, E. I.; Knyukshto, V. N.; Stasheuski, A. S.; Galievsky, V. A.; Stupak, A. P.; Blaudeck, T.; Borczyskowski, C. Quantitative Analysis of Singlet Oxygen ($^1O_2$) Generation via Energy Transfer in Nanocomposites Based on Semiconductor Quantum Dots and Porphyrin Ligands. *J. Phys. Chem. C* **2011**, *115*, 21535−21545.
(36) Charron, G.; Stuchinskaya, T.; Edwards, D. R.; Russell, D. A.; Nann, T. Insights into the Mechanism of Quantum Dot-Sensitized Singlet Oxygen Production for Photodynamic Therapy. *J. Phys. Chem. C* **2012**, *116*, 9334−9342.
(37) Pong, B. K.; Trout, B. L.; Lee, J. Y. Modified Ligand-Exchange for Efficient Solubilization of CdSe/ZnS Quantum Dots in Water: a Procedure Guided by Computational Studies. *Langmuir* **2008**, *24*, 5270−5276.
(38) Janczewski, D.; Tomczak, N.; Han, M. Y.; Vancso, G. J. Synthesis of Functionalized Amphiphilic Polymers for Coating Quantum Dots. *Nat. Protoc.* **2011**, *6*, 1546−1553.
(39) Lees, E. E.; Nguyen, T.; Clayton, A. H. A.; Mulvaney, P. The Preparation of Colloidally Stable, Water-Soluble, Biocompatible, Semiconductor Nanocrystals with a Small Hydrodynamic Diameter. *ACS Nano* **2009**, *3*, 1121−1128.
(40) Nann, T. Phase-transfer of CdSe@ZnS quantum dots using amphiphilic hyperbranched polyethylenimine. *Chem. Commun.* **2005**, *13*, 1735−1736.
(41) Sperling, R. A.; Parak, W. J. Surface Modification, Functionalization and Bioconjugation of Colloidal Inorganic Nanoparticles. *Philos. Trans. R. Soc., A* **2010**, *368*, 1333.
(42) Kelf, T. A.; Sreenivasan, V. K. A.; Sun, J.; Kim, E. J.; Goldys, E. M.; Zvyagin, A. V. Non-Specific Cellular Uptake of Surface-Functionalized Quantum Dots. *Nanotechnology* **2010**, *21*, 28.
(43) Carbone, L.; Nobile, C.; De Giorgi, M.; Sala, F. D.; Morello, G.; Pompa, P.; Hytch, M.; Snoeck, E.; Fiore, A.; Franchini, I. R.; Nadasan, M.; Silvestre, A. F.; Chiodo, L.; Kudera, S.; Cingolani, R.; Krahne, R.; Manna, L. Synthesis and Micrometer-Scale Assembly of Colloidal CdSe/CdS Nanorods Prepared by a Seeded Growth Approach. *Nano Lett.* **2007**, *7*, 2942−2950.
(44) Dubertret, B.; Skourides, P.; Norris, D. J.; Noireaux, V.; Brivanlou, A. H.; Libchaber, A. In Vivo Imaging of Quantum Dots Encapsulated in Phospholipid Micelles. *Science* **2002**, *298*, 1759−1762.
(45) Roslaniec, M.; Weitman, H.; Freeman, D.; Mazur, Y.; Ehrenberg, B. Liposome Binding Constants and Singlet Oxygen Quantum Yields of Hypericin, Tetrahydroxy Helianthrone and Their Derivatives: Studies in Organic Solutions and in Liposomes. *J. Photochem. Photobiol., B* **2000**, *57*, 149−158.
(46) *Principles of Fluorescence Spectroscopy*; Lakowicz, J. R., 13th ed.; Springer Science & Business Media: New York, 2006; pp 443−476.
(47) Ben Dror, S.; Bronshtein, I.; Weitman, H.; Smith, K. M.; O'Neal, W. G.; Jacobi, P. A.; Ehrenberg, B. The Binding of Analogs of Porphyrins and Chlorins with Elongated Side Chains to Albumin. *Eur. Biophys. J.* **2009**, *38*, 847−855.
(48) Salant, A.; Shalom, M.; Tachan, Z.; Buhbut, S.; Zaban, A.; Banin, U. Quantum Rod-Sensitized Solar Cell: Nanocrystal Shape Effect on the Photovoltaic Properties. *Nano Lett.* **2012**, *12*, 2095−2100.
(49) Halivni, S.; Sitt, A.; Hadar, I.; Banin, U. Effect of Nanoparticle Dimensionality on Fluorescence Resonance Energy Transfer in Nanoparticle−Dye Conjugated Systems. *ACS Nano* **2012**, *6*, 2758−2765.
(50) *Poly (ethanol glycol) Chemistry: Biotechnical and Biomedical Applications*; Harris, J. M., Eds.; Plenum Press: New York and London, 1992.
(51) Tong, S.; Hou, S.; Ren, B.; Zheng, Z.; Bao, G. Self-Assembly of Phospholipid-PEG Coating on Nanoparticles Through Dual Solvent Exchange. *Nano Lett.* **2011**, *11*, 3720−3726.
(52) Lavi, A.; Weitman, H.; Holmes, R. T.; Smith, K. M.; Ehrenberg, B. The Depth of Porphyrin in a Membrane and the Membrane's Physical Properties Affect the Photosensitizing Efficiency. *Biophys. J.* **2002**, *82*, 2101−2110.

DOI: 10.1021/acsami.5b04318
ACS Appl. Mater. Interfaces 2015, 7, 21107−21114